nature medicine

Asfotase-α improves bone growth, mineralization and strength in mouse models of neurofibromatosis type-1

Jean de la Croix Ndong[1,2], Alexander J Makowski[1,3–5], Sasidhar Uppuganti[1,4], Guillaume Vignaux[1,2], Koichiro Ono[1,2,6], Daniel S Perrien[1,4,5,7], Simon Joubert[8], Serena R Baglio[9], Donatella Granchi[9], David A Stevenson[10], Jonathan J Rios[11–14], Jeffry S Nyman[1,3–5] & Florent Elefteriou[1,2,15,16]

Individuals with neurofibromatosis type-1 (NF1) can manifest focal skeletal dysplasias that remain extremely difficult to treat. NF1 is caused by mutations in the *NF1* gene, which encodes the RAS GTPase–activating protein neurofibromin. We report here that ablation of *Nf1* in bone-forming cells leads to supraphysiologic accumulation of pyrophosphate (PP_i), a strong inhibitor of hydroxyapatite formation, and that a chronic extracellular signal–regulated kinase (ERK)-dependent increase in expression of genes promoting PP_i synthesis and extracellular transport, namely *Enpp1* and *Ank*, causes this phenotype. *Nf1* ablation also prevents bone morphogenic protein-2–induced osteoprogenitor differentiation and, consequently, expression of alkaline phosphatase and PP_i breakdown, further contributing to PP_i accumulation. The short stature and impaired bone mineralization and strength in mice lacking *Nf1* in osteochondroprogenitors or osteoblasts can be corrected by asfotase-α enzyme therapy aimed at reducing PP_i concentration. These results establish neurofibromin as an essential regulator of bone mineralization. They also suggest that altered PP_i homeostasis contributes to the skeletal dysplasias associated with NF1 and that some of the NF1 skeletal conditions could be prevented pharmacologically.

© 2014 Nature America, Inc. All rights reserved.

Mutations in the *NF1* gene cause NF1, a genetic disorder with an incidence of 1/3,500 live births worldwide. This condition is characterized by malignant and nonmalignant pathologies, including skeletal manifestations[1–6]. Dystrophic scoliosis, tibia bowing, bone fragility, fracture and pseudarthrosis (nonunion following fracture) are skeletal conditions associated with high morbidity in this population[7–10]. Despite recent progress toward understanding the role of *NF1* in skeletal tissues, it is still unclear why and how these bone pathologies arise, raising uncertainty regarding optimal treatment[2,3].

Although individuals with NF1 are typically born with heterozygous mutations in *NF1*, loss of heterozygosity has been detected in pseudarthrosis biopsies[11], suggesting that local somatic *NF1* loss of function contributes to NF1 skeletal dysplasia. This point is further supported by the relative commonality of defects observed between pseudarthrosis lesions from individuals with NF1 and the skeleton of mice characterized by conditional loss of *Nf1* in osteoprogenitors. These mice indeed tend to recapitulate, in their entire skeleton, the genetic and cellular consequences of *NF1* loss of function that occurs locally in human NF1 pseudarthroses. *Nf1* inactivation in osteochondroprogenitors in $Nf1^{flox/flox}$; *Prx-cre* or $Nf1^{flox/flox}$; *Col2a1-cre* mice (herein called *Prx-Nf1* KO or *Col2-Nf1* KO mice, respectively) led to reduced stature, low bone mass, tibia bowing, diaphyseal ectopic blood vessel formation and hypomineralization associated with weakened bone mechanical properties. Bone cellular parameters also indicated that neurofibromin is required for normal osteoblast differentiation and expression of *Tnfsf11*, the gene encoding receptor activator of nuclear factor κB ligand, and hence for osteoclastogenesis[12–18]. The existence of *Nf1*-deficient osteoblasts in an *Nf1* heterozygous bone microenvironment has also been shown to cause bone loss and delayed bone healing in $Nf1^{flox/flox}$; *Col1a1-cre* (*Col1-Nf1* KO) mice via activation of transforming growth factor-β (TGF-β) signaling[19]. Notably, each of these NF1 models, as well as bone biopsies from individuals with NF1 pseudarthrosis[20], are characterized by excessive deposition of unmineralized bone matrix (osteoid) despite normal serum phosphate and calcium concentrations.

Bone matrix mineralization is a tightly regulated process that requires collagen, calcium and phosphate to form ordered crystals of hydroxyapatite, as well as tissue-nonspecific alkaline phosphatase

[1]Vanderbilt Center for Bone Biology, Vanderbilt University Medical Center, Nashville, Tennessee, USA. [2]Department of Medicine, Vanderbilt University Medical Center, Nashville, Tennessee, USA. [3]Department of Biomedical Engineering, Vanderbilt University, Nashville, Tennessee, USA. [4]Department of Orthopaedic Surgery & Rehabilitation, Vanderbilt University Medical Center, Nashville, Tennessee, USA. [5]Department of Veterans Affairs, Tennessee Valley Healthcare System, Nashville, Tennessee, USA. [6]Department of Orthopaedics, Nohon Koukan Hospital, Kawasaki, Kanagawa, Japan. [7]Vanderbilt University Institute of Imaging Sciences, Vanderbilt University Medical Center, Nashville, Tennessee, USA. [8]Alexion Pharmaceuticals, Cheshire, Connecticut, USA. [9]Laboratory for Orthopedic Pathophysiology and Regenerative Medicine, Istituto Ortopedico Rizzoli, Bologna, Italy. [10]Department of Pediatrics, University of Utah, Salt Lake City, Utah, USA. [11]Sarah M. and Charles E. Seay Center for Musculoskeletal Research, Texas Scottish Rite Hospital for Children, Dallas, Texas, USA. [12]Department of Pediatrics, UT Southwestern Medical Center, Dallas, Texas, USA. [13]Eugene McDermott Center for Human Growth & Development, UT Southwestern Medical Center, Dallas, Texas, USA. [14]Department of Orthopaedic Surgery, UT Southwestern Medical Center, Dallas, Texas, USA. [15]Department of Pharmacology, Vanderbilt University Medical Center, Nashville, Tennessee, USA. [16]Department of Cancer Biology, Vanderbilt University Medical Center, Nashville, Tennessee, USA. Correspondence should be addressed to F.E. (florent.elefteriou@vanderbilt.edu).

Received 12 December 2013; accepted 1 May 2014; published online 6 July 2014; doi:10.1038/nm.3583

(ALP) activity to hydrolyze PP_i (a potent inhibitor of mineralization) and generate inorganic phosphate[21]. Extracellular concentrations of PP_i are determined by (i) its degradation via ALP, (ii) its synthesis catalyzed by the nucleoside triphosphate pyrophosphohydrolase ENPP1/PC-1 (called ENPP1 herein) and (iii) its transport into the extracellular milieu through the PP_i channel ANK[22]. Mineralization is also controlled by Phospho1, a phosphatase that provides intracellular inorganic phosphate to generate PP_i[23], and by glycoproteins such as osteopontin, which inhibits crystal nucleation on collagen fibers in mineralizing vesicles[24,25]. Multiple growth factors such as TGF-β, activin A, bone morphogenic protein-2 (BMP2), insulin-like growth factor-1, fibroblast growth factor-2 and fibroblast growth factor-23 are involved in bone and/or cartilage mineralization[26–34]. A common signaling pathway engaged by these factors is the RAS-ERK pathway, which is constitutively activated in cells lacking neurofibromin, the RAS GTPase–activating protein (RAS-GAP) encoded by *NF1* (ref. 35). We thus hypothesized that neurofibromin, via its inhibitory action on RAS-ERK signaling in bone-forming cells, could be an important regulator of bone matrix mineralization and bone mechanical properties. We show here that neurofibromin inhibits the expression of genes increasing PP_i extracellular levels and that hydrolysis of excess PPi with a recombinant form of ALP improves bone growth and mineralization in mouse models of NF1 skeletal dysplasia. These data suggest a potential pharmacological avenue to prevent some of the skeletal abnormalities of individuals with NF1.

RESULTS

Uncontrolled PP_i production in *Nf1*-deficient bone cells

To address whether and how *Nf1* regulates bone mineralization, we first asked whether *Nf1* ablation in bone marrow stromal cells (BMSCs) affects extracellular PP_i concentrations. BMSCs from *Col2-Nf1* KO mice, lacking *Nf1* in osteochondroprogenitor cells, showed a 60–70% lower *Nf1* expression compared to those from wild-type (WT) mice (**Fig. 1a**), consistent with the heterogeneous nature of the cell populations that comprise BMSC cultures[36]. This lower *Nf1* expression level was accompanied by a significantly higher (70%) extracellular PP_i concentration in the conditioned medium of undifferentiated BMSC cultures compared to that of WT controls (**Fig. 1b**). Addition of a recombinant form of ALP, in the form of sALP-FcD10 (also known as asfotase-α, 0.5 μg ml^{-1}) to induce PP_i hydrolysis significantly reduced the amount of PP_i detected in both genotypes, confirming the validity of the PP_i measurements.

High extracellular PP_i concentration can be generated by increased production of PP_i by the ectonucleophosphatase ENPP1 and by increased cellular export through the transporter ANK. Both *Ank* and *Enpp1* mRNA (**Fig. 1c**) and protein (**Supplementary Fig. 1a**) levels were higher in *Nf1*-deficient BMSCs compared to WT BMSCs. Expression of the gene encoding osteopontin (*Spp1*) was also higher in *Nf1*-deficient BMSCs (**Fig. 1c**), consistent with the reported stimulatory effect of PP_i on *Spp1* expression[25]. We obtained similar results when comparing *Nf1*-deficient osteoprogenitor cells generated from $Nf1^{flox/flox}$ BMSC cultures infected with a Cre-expressing adenovirus to control $Nf1^{flox/flox}$ BMSC cultures infected with a GFP-expressing adenovirus (**Supplementary Fig. 1b**), which confirmed that the changes in gene expression measured in BMSCs from *Col2-Nf1* KO mice were not caused by fewer osteoprogenitors initially plated. *Ank*, *Enpp1* and *Spp1* expression was also significantly higher in long bones, calvarias and epiphyses (cartilage) from 3-week-old *Col2-Nf1* KO versus WT mice (**Fig. 1d**), whereas expression of *Runx2* and *Alpl*, two osteoblast differentiation marker genes, was lower (**Supplementary Fig. 1c**). Lastly, MEK inhibition by U0126 (1 μM, 24 h) blunted the increase in *Ank*, *Enpp1* and *Spp1* expression observed in *Nf1*-deficient BMSCs, indicating that neurofibrin controls the expression of these genes in a RAS/ERK-dependent fashion (**Fig. 1c** and **Supplementary Fig. 1b**).

To assess whether these molecular findings in mice could be replicated in humans, we obtained RNA from adherent human bone stromal cells prepared from bone biopsies from six healthy control subjects without NF1 and nine individuals with NF1 tibial pseudarthrosis, and measured *ENPP1* and *ANKH* transcript levels by quantitative PCR. Consistent with the mouse data, *ENPP1* expression was significantly higher in cultured cells from NF1 pseudarthrosis tissues (**Fig. 1e**), despite the small number of available samples and consistent with the cell heterogeneity of these cultures. *ANKH* expression, however,

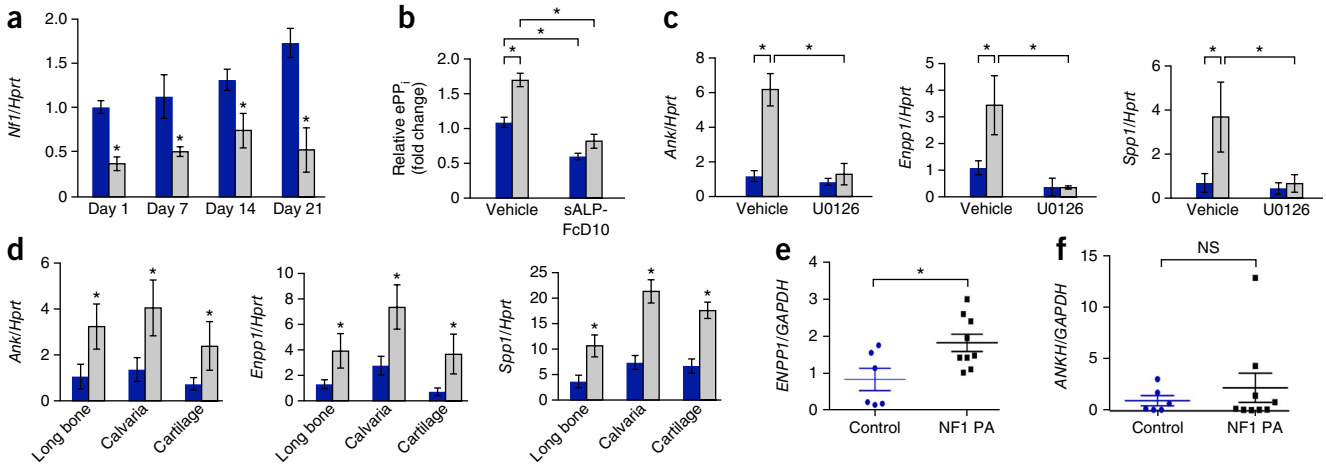

Figure 1 Uncontrolled *Ank*, *Enpp1* and *Spp1* expression and increased PP_i production in *Nf1*-deficient osteoblasts. (**a**) *Nf1* mRNA expression in mouse BMSCs differentiated for 7, 14 and 21 d ($n = 3$). (**b**) Extracellular PP_i (ePP_i) concentration in the conditioned medium of undifferentiated BMSCs ($n = 3$). Vehicle, $Na(PO_4)^{2-}$, pH 7.4. (**c**) *Ank*, *Enpp1* and *Spp1* mRNA expression in BMSCs treated with vehicle (DMSO) or U0126 for 24 h ($n = 3$). (**d**) *Ank*, *Enpp1* and *Spp1* mRNA expression in long bones, calvarias and epiphyses of 3-week-old WT (blue) and *Col2-Nf1* KO (gray) mice ($n = 6$ per group). (**e**,**f**) *ENPP1* and *ANKH* mRNA expression in human adherent bone marrow cells from control ($n = 6$ per group) and NF1-related pseudarthrosis (NF1 PA, $n = 9$ per group) biopsies. $^*P < 0.05$, determined by one-way analysis of variance (ANOVA) and Student's *t*-test. NS, nonsignificant. Data are expressed as mean ± s.d.

© 2014 Nature America, Inc. All rights reserved.

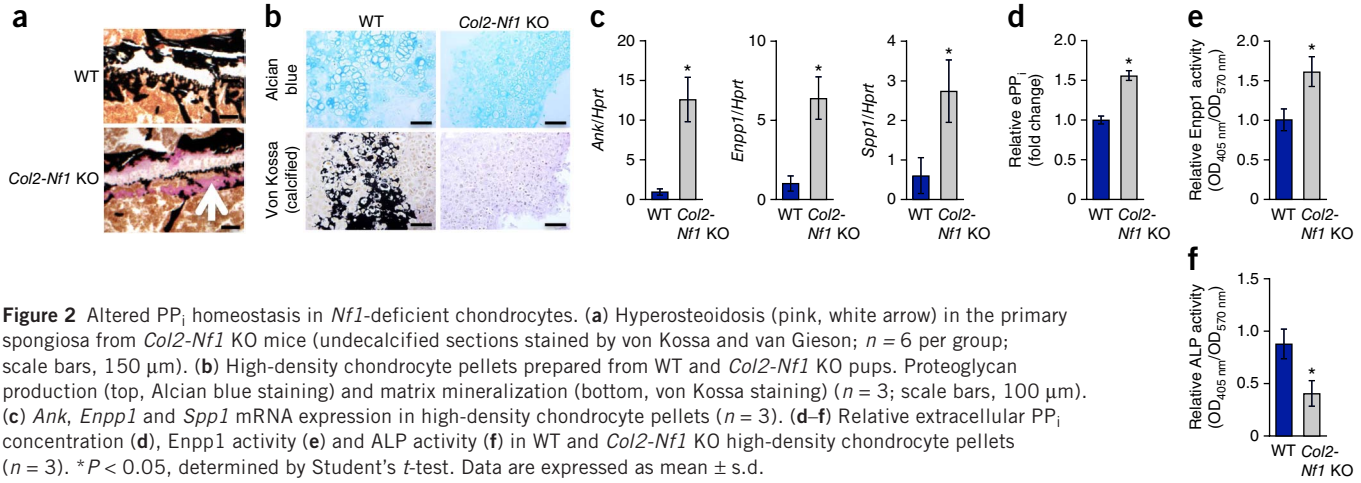

Figure 2 Altered PP_i homeostasis in *Nf1*-deficient chondrocytes. (**a**) Hyperosteoidosis (pink, white arrow) in the primary spongiosa from *Col2-Nf1* KO mice (undecalcified sections stained by von Kossa and van Gieson; $n = 6$ per group; scale bars, 150 µm). (**b**) High-density chondrocyte pellets prepared from WT and *Col2-Nf1* KO pups. Proteoglycan production (top, Alcian blue staining) and matrix mineralization (bottom, von Kossa staining) ($n = 3$; scale bars, 100 µm). (**c**) *Ank*, *Enpp1* and *Spp1* mRNA expression in high-density chondrocyte pellets ($n = 3$). (**d**–**f**) Relative extracellular PP_i concentration (**d**), Enpp1 activity (**e**) and ALP activity (**f**) in WT and *Col2-Nf1* KO high-density chondrocyte pellets ($n = 3$). $^*P < 0.05$, determined by Student's *t*-test. Data are expressed as mean ± s.d.

was variable between samples and not significantly different between cultures from normal and NF1 pseudarthrosis biopsies (**Fig. 1f**).

Mice lacking *Nf1* in mature osteoblasts (*Col1-Nf1* KO mice) have a uniform distribution of nonmineralized matrix throughout trabecular bone compartments[18], whereas mice lacking *Nf1* in osteochondroprogenitors and chondrocytes (*Col2-Nf1* KO mice) are characterized by an osteoid preferentially distributed in the primary spongiosa, where osteoblasts and chondrocytes mineralize their matrix (**Fig. 2a**). On the basis of these observations and because neurofibromin is expressed in hypertrophic chondrocytes[37,38], we hypothesized that this RAS-GAP could also contribute to cartilage mineralization, which is a process important for bone growth and ossification during development and bone healing in adults. In support of this hypothesis, *Col2-Nf1* KO chondrocyte high-density micromass cultures generated a typical Alcian blue–positive matrix but did not show signs of mineralization, in contrast to WT chondrocyte cultures (**Fig. 2b**). In addition, *Ank*, *Enpp1* and *Spp1* expression was significantly higher in *Nf1*-deficient micromass chondrocyte cultures versus WT cultures (**Fig. 2c**), in agreement with the data obtained from cartilaginous epiphyses, which contain a high proportion of chondrocytes (**Fig. 1d**). Accordingly, extracellular PP_i concentration (**Fig. 2d**) and Enpp1 enzymatic activity (**Fig. 2e**) were significantly higher, whereas ALP activity was lower (**Fig. 2f**) in *Nf1*-deficient versus WT chondrocytes.

Lack of *Nf1* in BMSCs impairs BMP2 osteogenic action

BMSCs isolated from *Col2-Nf1* KO mice displayed, compared to BMSCs isolated from WT mice, a significantly lower differentiation potential, as determined by lower osteoblast colony-forming unit (CFU-Ob) number, lower tissue-nonspecific ALP activity (**Fig. 3a**) and lower expression of osteoblast differentiation markers including *Runx2*, *Alpl* and *Bglap*, the gene encoding osteocalcin (**Fig. 3b**). We obtained similar results using $Nf1^{flox/flox}$ BMSCs infected with a Cre-expressing adenovirus (**Supplementary Fig. 1d**,**e**). However, in contrast to what we observed in the case of *Ank* and *Enpp1* expression, MEK inhibition by U0126 (1 µM), tremetinib or PD198306 (0.1 µM and 200 nM, respectively, data not shown) for 24 h did not correct the expression level of *Runx2* or *Alpl* in *Nf1*-deficient BMSCs (**Fig. 3c**), indicating that the expression of these two genes is not directly controlled by neurofibromin. Extracellular PP_i concentration, as well as *Ank*, *Enpp1* and *Spp1* expression, remained above or equal to that of WT controls throughout the differentiation period (**Fig. 3d**,**e**).

BMPs are known for their ability to promote osteoprogenitor differentiation[39] but have had limited effects on the differentiation of *Nf1*-heterozygous osteoprogenitors and on bone union in *Nf1*-heterozygous mice[40,41]. Recombinant human BMP2 (100 ng ml^{-1}) did not stimulate ALP activity or CFU-Ob formation in BMSC cultures from *Col2-Nf1* KO mice, although it did, as expected, promote

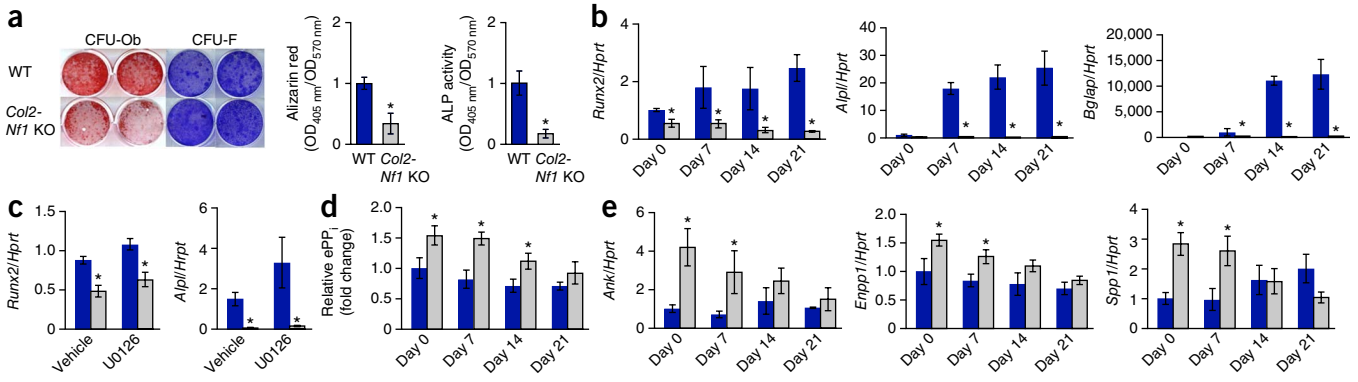

Figure 3 Blunted BMP2 response and osteoblast differentiation potential in *Nf1*-deficient osteoprogenitors. (**a**) BMSC differentiation analyzed by Alizarin red S staining (differentiation and mineralization, CFU-Ob), crystal violet staining of fibroblast CFUs (cell number, CFU-F, left), soluble Alizarin red S/crystal violet optical density ratio (middle) and ALP activity/crystal violet ratio (right) ($n = 3$). Blue, WT mice; gray, *Col2-Nf1* KO mice. (**b**) *Runx2*, *Alpl* and *Bglap* mRNA expression in BMSCs differentiated for 7, 14 and 21 d ($n = 3$). (**c**) *Runx2* and *Alpl* mRNA expression in serum-starved BMSCs treated with vehicle (DMSO) or U0126 for 24 h ($n = 3$). (**d**) Extracellular PP_i concentration/protein concentration in BMSCs differentiated for 7, 14 and 21 d ($n = 3$). (**e**) Normalized *Ank*, *Enpp1* and *Spp1* mRNA expression in BMSCs differentiated for 7, 14 and 21 d ($n = 3$). $^*P < 0.05$, determined by one-way ANOVA and Student's *t*-test. Data are expressed as mean ± s.d.

© 2014 Nature America, Inc. All rights reserved.

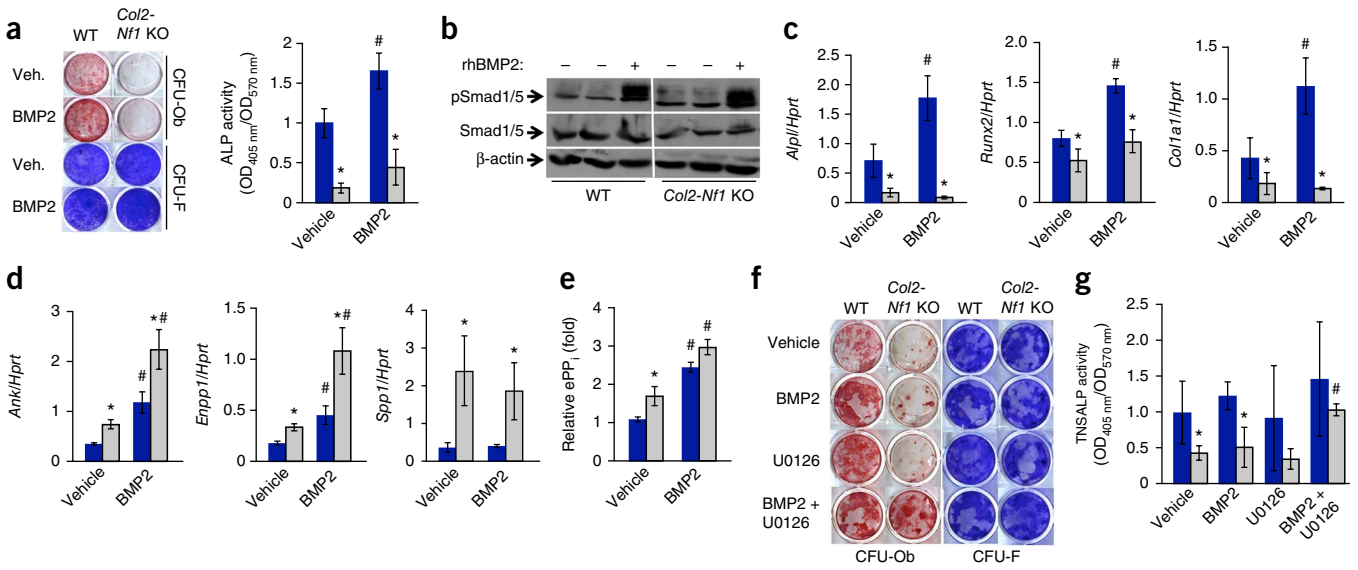

Figure 4 BMP2 does not promote differentiation in *Nf1*-deficient BMSCs but exacerbates their mineralization deficit. (**a**) BMSC differentiation analyzed by Alizarin red S (differentiation and mineralization, CFU-Ob) and crystal violet (cell number, CFU-F) staining ($n = 3$) and ALP activity ($n = 3$) following vehicle (Veh.) or BMP2 treatment. Blue, WT mice; gray, *Nf1* KO mice. (**b**) Phosphorylated Smad1 and/or Smad5 (pSmad1/5) induction in serum-starved BMSCs following recombinant human BMP2 (rhBMP2) treatment for 1 h. Smad1/5 and β-actin served as loading controls ($n = 3$). (**c**,**d**) *Alpl*, *Runx2* and *Col1a1* (**c**) and *Ank*, *Enpp1* and *Spp1* (**d**) mRNA expression following BMP2 treatment for 2 weeks ($n = 3$). (**e**) Extracellular PP_i relative concentration (normalized to protein concentration) in the conditioned medium of BMSCs treated with BMP2 for 24 h ($n = 3$). (**f**,**g**) BMSC differentiation analyzed by Alizarin red S (differentiation and mineralization, CFU-Ob) and crystal violet (cell number, CFU-F) staining (**f**, $n = 3$) and ALP activity (**g**, $n = 3$) following treatment with vehicle or BMP2 or U0126 or both for 2 weeks. $^*P < 0.05$ versus WT in the same treatment group; $^\#P < 0.05$ versus vehicle in the same genotype group, determined by one-way ANOVA and Student's *t*-test. Data are expressed as mean ± s.d.

CFU-Ob formation and ALP activity in WT BMSC cultures following 2 weeks of treatment (**Fig. 4a**). Smad1 and Smad5 phosphorylation in response to BMP2 treatment (100 ng ml^{-1}, 1 h) was not affected by *Nf1* deficiency (**Fig. 4b**), indicating that the lack of stimulatory effect of BMP2 on *Nf1*-deficient BMSC differentiation is not caused by repression of BMP2 receptor expression or by the production of factors inhibiting canonical Smad signaling. Treatment with BMP2 for 2 weeks also failed to increase the expression of *Alpl*, *Runx2* and *Col1a1* in BMSC cultures from *Col2-Nf1* KO mice (**Fig. 4c**). However, it significantly increased the expression of *Ank* and *Enpp1* (but not *Spp1*) (**Fig. 4d**) and PP_i extracellular concentration (**Fig. 4e**) in both WT and *Nf1*-deficient BMSCs. CFU-Ob formation, ALP activity (**Fig. 4f**,**g**) and the expression of *Alpl* and *Col1a1* (**Supplementary Fig. 2a**,**b**) in *Nf1*-deficient BMSC cultures were higher following a 2-week-long combined treatment with the MEK inhibitor U0126 (1 μM) and BMP2 (100 ng ml^{-1}), but not with either of these treatments alone. This combination treatment also partially reduced the increased *Ank* and *Enpp1* expression and PP_i extracellular concentration detected in vehicle-treated *Nf1*-deficient BMSC cultures, possibly owing to the antagonistic effect of these two drugs on *Ank* and *Enpp1* expression (**Supplementary Fig. 2c**,**d**).

sALP-FcD10 improves bone growth and mineral density in *Col2-Nf1* KO mice

If excessive extracellular PP_i levels cause the mineralization deficit observed in *Col2-Nf1* KO mice, then reducing PP_i concentration should have beneficial effects on matrix mineralization. This is experimentally possible by inhibiting PP_i generation or increasing its catabolism. We chose the latter approach because PP_i is a substrate for ALP, and a recombinant form of human ALP is clinically available to treat *ALPL*-deficient subjects with hypophosphatasia[42,43]. We thus treated WT and *Nf1*-deficient BMSCs with vehicle or sALP-FcD10 (0.5 mg ml^{-1}) in osteogenic conditions for 14 d and assessed matrix mineralization. As predicted, sALP-FcD10 increased matrix mineralization in both genotypes, although the relative increase was more pronounced in cultures from *Col2-Nf1* KO than in those from WT mice (**Fig. 5a**). This pronounced increase occurred despite the persistent differentiation deficit of *Nf1*-deficient BMSCs in the presence of sALP-FcD10 (**Supplementary Fig. 3a**). Treatment with sALP-FcD10 reduced *Spp1* expression in *Nf1*-deficient BMSCs (**Supplementary Fig. 3a**), in agreement with the known stimulatory effect of PP_i on *Spp1* expression[25].

On the basis of these encouraging results, we treated *Col2-Nf1* KO newborn mice daily with subcutaneous injections of sALP-FcD10 (8.2 mg per kg body weight per d) for 18 d[44,45]. *Col2-Nf1* KO mice have short stature, low bone mass, decreased bone mineralization, cortical thickness and mineral density, and high cortical porosity[37]. Following this short treatment (dictated by the relatively high death rate of these mice at weaning), we observed a significant 73% increase in the size of mutant mice (**Fig. 5b**) and a clear increase in vertebral and tibial bone mineral density on radiographs (**Fig. 5c**,**d**). Treatment with sALP-FcD10 also significantly increased mid-diaphyseal cortical bone thickness, as measured by three-dimensional microcomputed tomography (μCT) (**Fig. 5e**), partially rescued the formation of secondary ossification centers, expanded tibia metaphyseal envelopes and increased the amount of calcified matrix in the growth plate hypertrophic zone of *Col2-Nf1* KO mice (**Fig. 5f**). Despite the seemingly pronounced effects of sALP-FcD10 observed by radiography and μCT, tibia cortical tissue mineral density and mineral-to-collagen ratio (**Supplementary Fig. 3b**,**c**) were not increased following treatment.

sALP-FcD10 increases bone mineralization in *Osx-Nf1* KO mice

Because *Col2-Nf1* KO mice manifest severe developmental phenotypes that limit their survival and thus the duration of treatments,

© 2014 Nature America, Inc. All rights reserved.

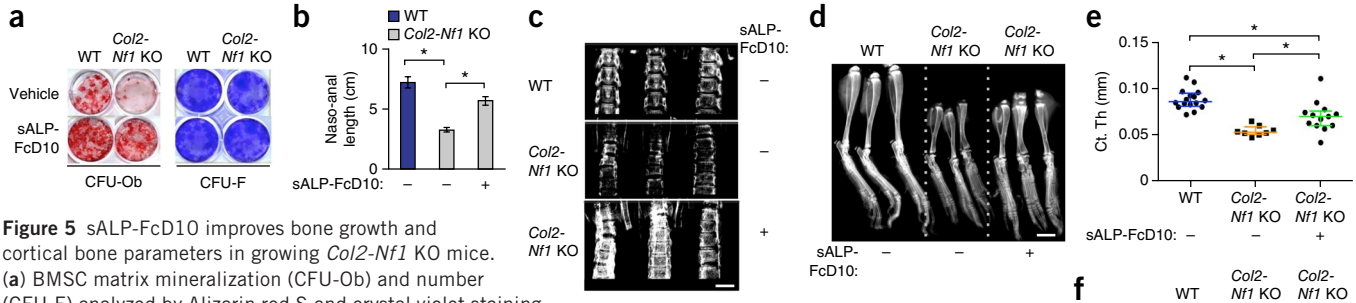

sALP-FcD10:	–	–	+
hBV/TV (%)	0.481 ± 0.1	0.340 ± 0.12*	0.548 ± 0.09#

Figure 5 sALP-FcD10 improves bone growth and cortical bone parameters in growing *Col2-Nf1* KO mice. (**a**) BMSC matrix mineralization (CFU-Ob) and number (CFU-F) analyzed by Alizarin red S and crystal violet staining, respectively ($n = 3$), following vehicle or sALP-FcD10 treatment for 2 weeks. (**b**–**f**) Bone growth (**b**, naso-anal length; WT, $n = 14$, KO + vehicle, $n = 8$, KO + sALP-FcD10, $n = 13$; P value determined by one-way ANOVA), vertebral (**c**, scale bar, 250 µm; WT, $n = 14$, KO + vehicle, $n = 8$, KO + sALP-FcD10, $n = 13$; P value determined by one-way ANOVA) and tibial (**d**, scale bar, 250 µm; WT, $n = 14$, KO + vehicle, $n = 8$, KO + sALP-FcD10, $n = 13$; P value determined by one-way ANOVA), bone mineral density (X-rays), cortical thickness (**e**, Ct.Th, µCT; WT, $n = 16$, KO + vehicle, $n = 8$, KO + sALP-FcD10, $n = 13$; P value determined by one-way ANOVA with Holm-Sidak's method), epiphyseal diameter (**f**, white arrows; scale bar, 45 µm; µCT) and hypertrophic zone von Kossa–positive calcified bone volume/tissue volume (hBV/TV, histology; WT, $n = 7$, KO + vehicle, $n = 6$, KO + sALP-FcD10, $n = 7$; P value determined by one-way ANOVA) in *Col2-Nf1* KO newborn pups treated daily with sALP-FcD10 for 18 d. *$P < 0.05$ versus WT; #$P < 0.05$ versus vehicle in the same genotype group. Data are expressed as mean ± s.d.

we generated mice in which *Nf1* can be ablated postnatally in osteoprogenitors expressing *Sp7* (also known as *Osx*) by crossing the inducible Tet-Off–based *Osx-cre* transgenic mice[46] with $Nf1^{flox/flox}$ mice[47]. This new mouse model makes it possible to dissect the mechanisms by which postnatal *Nf1* ablation impairs bone homeostasis, without complications arising from developmental phenotypes. *Osx-cre*; $Nf1_{Osx}^{flox/flox}$ mice (herein called *Osx-Nf1* KO mice) were undistinguishable in size from WT littermates upon doxycycline administration (i.e., Cre recombinase repression) from conception to day 14 (**Fig. 6a**) and had normal phosphate, calcium and 25-hydroxycholecalciferol (vitamin D) serum concentrations (**Supplementary Table 1**). *Osx-cre*–mediated *Nf1* ablation in osteoprogenitors at postnatal day 14 following doxycycline withdrawal, as seen in *Col2-Nf1* KO mice, caused hyperosteoidosis (**Fig. 6b**), lower bone mass (**Fig. 6c**), higher femoral diaphyseal cortical porosity (**Fig. 6d**) and lower cortical thickness, midshaft moment of inertia and cortical tissue mineral density compared to WT mice (**Fig. 6e**–**g**). Cortical mineral-to-collagen ratio measured by Raman spectroscopy (**Fig. 6h**)

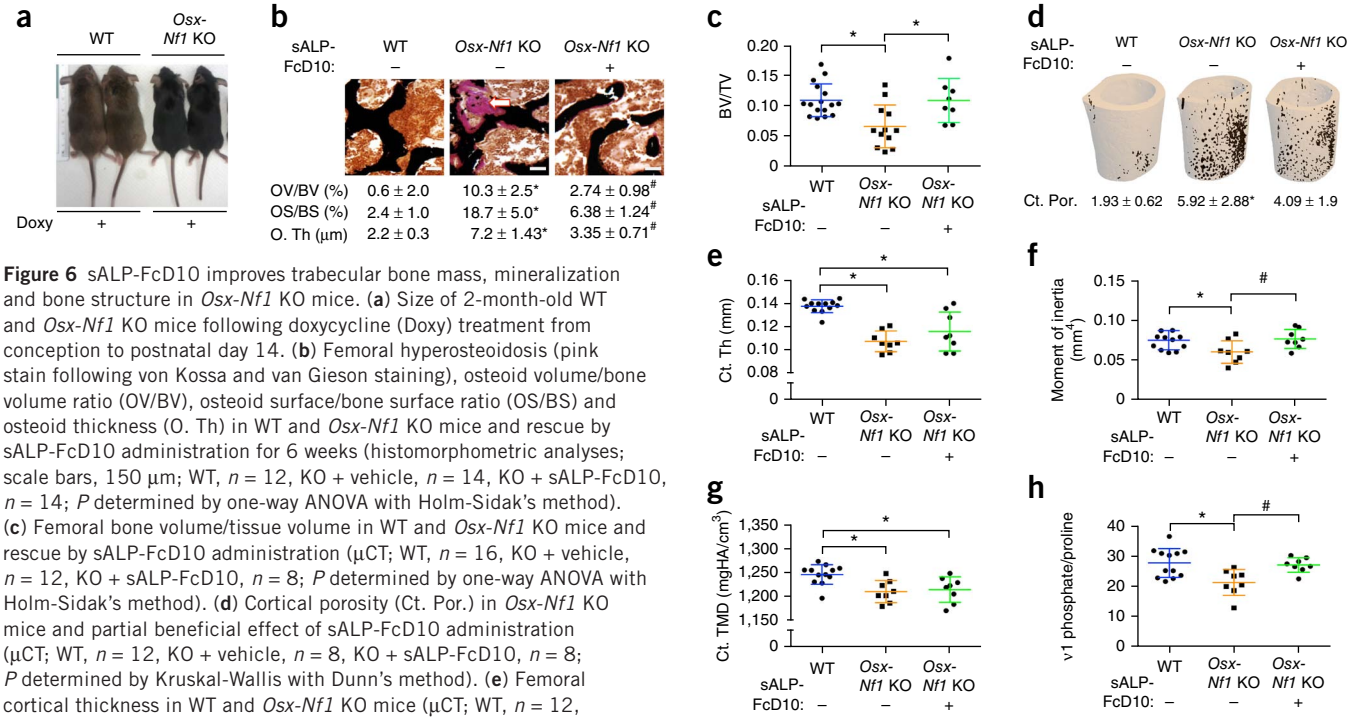

	WT	Osx-Nf1 KO	Osx-Nf1 KO
OV/BV (%)	0.6 ± 2.0	10.3 ± 2.5*	2.74 ± 0.98#
OS/BS (%)	2.4 ± 1.0	18.7 ± 5.0*	6.38 ± 1.24#
O. Th (µm)	2.2 ± 0.3	7.2 ± 1.43*	3.35 ± 0.71#

	WT	Osx-Nf1 KO	Osx-Nf1 KO
Ct. Por.	1.93 ± 0.62	5.92 ± 2.88*	4.09 ± 1.9

Figure 6 sALP-FcD10 improves trabecular bone mass, mineralization and bone structure in *Osx-Nf1* KO mice. (**a**) Size of 2-month-old WT and *Osx-Nf1* KO mice following doxycycline (Doxy) treatment from conception to postnatal day 14. (**b**) Femoral hyperosteoidosis (pink stain following von Kossa and van Gieson staining), osteoid volume/bone volume ratio (OV/BV), osteoid surface/bone surface ratio (OS/BS) and osteoid thickness (O. Th) in WT and *Osx-Nf1* KO mice and rescue by sALP-FcD10 administration for 6 weeks (histomorphometric analyses; scale bars, 150 µm; WT, $n = 12$, KO + vehicle, $n = 14$, KO + sALP-FcD10, $n = 14$; P determined by one-way ANOVA with Holm-Sidak's method). (**c**) Femoral bone volume/tissue volume in WT and *Osx-Nf1* KO mice and rescue by sALP-FcD10 administration (µCT; WT, $n = 16$, KO + vehicle, $n = 12$, KO + sALP-FcD10, $n = 8$; P determined by one-way ANOVA with Holm-Sidak's method). (**d**) Cortical porosity (Ct. Por.) in *Osx-Nf1* KO mice and partial beneficial effect of sALP-FcD10 administration (µCT; WT, $n = 12$, KO + vehicle, $n = 8$, KO + sALP-FcD10, $n = 8$; P determined by Kruskal-Wallis with Dunn's method). (**e**) Femoral cortical thickness in WT and *Osx-Nf1* KO mice (µCT; WT, $n = 12$, KO + vehicle, $n = 8$, KO + sALP-FcD10, $n = 8$; P determined by Kruskal-Wallis with Dunn's method). (**f**) Moment of inertia in WT and *Osx-Nf1* KO mice and rescue by sALP-FcD10 administration (µCT; WT, $n = 12$, KO + vehicle, $n = 8$, KO + sALP-FcD10, $n = 8$; P determined by one-way ANOVA with Holm-Sidak's method). (**g**) Cortical tissue mineral density (Ct. TMD) in WT and *Osx-Nf1* KO mice (µCT; WT, $n = 12$, KO + vehicle, $n = 8$, KO + sALP-FcD10, $n = 8$; P determined by one-way ANOVA with Holm-Sidak's method). (**h**) Mineral-to-collagen ratio (v1 phosphate/proline) in WT and *Osx-Nf1* KO mice and rescue by sALP-FcD10 administration (Raman spectroscopy; WT, $n = 12$, KO + vehicle, $n = 8$, KO + sALP-FcD10, $n = 8$; P determined by Kruskal-Wallis with Dunn's method). *$P < 0.05$ versus WT; #$P < 0.05$ versus vehicle in the same genotype group. Data are expressed as mean ± s.d.

© 2014 Nature America, Inc. All rights reserved.

was also lower in *Osx-Nf1* KO mice, and femurs from *Osx-Nf1* KO mice were mechanically weaker than those from WT controls, as measured by three-point bending tests (**Supplementary Table 2**).

To assess the effect of sALP-FcD10 on the skeleton of this mouse model, we administered sALP-FcD10 daily from 2 weeks of age (at the time of *Nf1* ablation) for 6 weeks. In *Osx-Nf1* KO mice, treatment with sALP-FcD10 significantly increased trabecular bone volume/tissue volume ratio and moment of inertia, as assessed by μCT (**Fig. 6c**,**f**), as well as femoral stiffness, modulus and peak force, as measured by three-point bending (**Supplementary Table 2**), and led to a non-significant trend for increased cortical femoral thickness (**Fig. 6e**). Treatment with sALP-FcD10 also improved bone mineralization in *Osx-Nf1* KO mice, as measured by a drastic 73% reduction in osteoid volume per bone volume, a 65% reduction in osteoid surface per bone surface, a 53% decrease in osteoid thickness (**Fig. 6b**) and a 20% increase in mineral-to-collagen ratio (**Fig. 6h**).

DISCUSSION

We show here that the RAS-GAP activity of neurofibromin in the bone mesenchymal lineage restrains the expression of *Enpp1* and *Ank*, two main genes controlling PP_i homeostasis, and that increasing PP_i catabolism through enzyme therapy considerably improves bone mineralization and bone mechanical properties in mouse models of NF1 skeletal dysplasia. These results, along with suggestive evidence of conservation of function between mice and humans, support the causal role of increased PP_i levels in the etiology of NF1-related hyperosteoidosis and position neurofibromin as a critical and obligatory regulator of cartilage and bone mineralization. They also provide preclinical evidence that some of the most clinically challenging NF1-related skeletal maladies might be preventable.

Hyperactive TGF-β signaling has been proposed to cause bone loss and to delay bone healing in mice deficient for *Nf1* in mature osteoblasts and heterozygous for *Nf1* (ref. 19). TGF-β is also known to stimulate ERK activity and *Ank* and *Enpp1* expression, and to increase PP_i concentration in WT chondrocytes[48,49]. Therefore, *NF1*-deficient BMSCs may contribute cell autonomously and/or in a hyperactive TGF-β paracrine fashion to the extraphysiological skeletal accumulation of PP_i and to the impaired osteoblast differentiation and matrix mineralization observed in the setting of NF1. The beneficial effect of sALP-FcD10 on bone growth, mineralization and strength observed in this study suggests that PP_i accumulation and abnormal mineralization are important components of NF1-related bone dysplasia. However, further studies will be necessary to determine the evolution and contribution of all the cellular defects typical of *Nf1*-deficient bone cells on bone mass and strength over extended periods of treatment with sALP-FcD10, as this drug does not correct the differentiation phenotype of *Nf1*-deficient osteoblasts. Although TGF-β blockade might theoretically be used to promote bone union in children with NF1 pseudarthrosis, the cancer-prone status of this pediatric population and the known tumor-suppressor activity of TGF-β signaling limit this therapeutic approach[50]. Our results, on the other hand, suggest that stimulation of PP_i catabolism through enzyme therapy could be applied on a more chronic basis before fracture to strengthen the NF1-related dysplastic bones and prevent their mechanical failure.

The mineralization deficit of *Nf1*-deficient BMSCs could be detected in immature BMSCs before their differentiation into osteoblasts. Therefore, this phenotype cannot be attributed to the reduced differentiation potential of *Nf1*-deficient BMSCs, although the latter certainly contributes to the low bone mass phenotype observed in the two NF1 mouse models used in this study. It is also worth noting that BMP2 treatment, without the need for ERK blockade, stimulated the expression of *Ank* and *Enpp1* and increased extracellular PP_i concentration in *Nf1*-deficient BMSC cultures, as shown previously in WT cells[28]. This observation could explain why recombinant human BMP2 alone did not improve bone healing in NF1 mouse models[40,41] and bone union in individuals with NF1-related pseudarthrosis[51–53].

Our results indicate that *Nf1*-deficient BMSCs are not responsive to BMP2 with regard to their differentiation potential and suggest that this defect may in part underlie their inability to differentiate. In addition, the response of *Nf1*-deficient BMSCs to BMP2 with regard to *Ank* and *Enpp1* expression suggests that neurofibromin is not the sole negative regulator of the RAS-ERK signaling pathway upstream of these two genes. These results also indicate that the stimulatory effect of BMP2 on osteoprogenitor differentiation requires controlled ERK signaling by neurofibromin.

It is unknown to what extent poor matrix mineralization contributes to the low bone mineral density, tibia bowing, poor mechanical properties and possibly pseudarthrosis observed in children with NF1. Although local PP_i concentration could not be quantified, the observed increase in the expression of *ENPP1* in BMSCs extracted from biopsies of pseudarthroses from patients with NF1, as well as the presence of thick osteoid seams on histological sections[20], supports conservation of function between mice and humans.

Pseudarthrosis and dystrophic scoliosis can currently be treated only by invasive, and often repetitive, surgical orthopedic interventions[2,3]. Most approaches to date are corrective in nature, and only bracing techniques are available to reduce the incidence and severity of these complications. Of major interest is the possibility that sALP-FcD10, if applied preventatively, might improve mineralization, growth, architecture and mechanical properties of dysplastic bones affected by NF1 and, thus, limit their likelihood of deformation and fracture. This latter point is particularly noteworthy, as the current standard for treatment is limited to avoidance of prophylactic surgery and early long-term bracing to prevent fracture until skeletal maturity is reached. It is worth emphasizing that sALP-FcD10 targets bone and is already successfully used in the clinic to treat children with hypophosphatasia[42]. Therefore, its potential use in the context of NF1-related skeletal dysplasia has an advantage over the development of other experimental drugs that target this and other aspects of the NF1 skeletal pathologies.

METHODS

Methods and any associated references are available in the online version of the paper.

Note: Any Supplementary Information and Source Data files are available in the online version of the paper.

ACKNOWLEDGMENTS

We thank A. Bianchi and F. Cailotto for their help in establishing the PP_i measurement protocol and K.S. Campbell for editorial assistance. This work was supported by a Young Investigator Award (2012–01–028) from the Children's Tumor Foundation (J.d.l.C.N.), the US National Institute of Arthritis and Musculoskeletal and Skin Diseases and National Center for Research Resources, part of the US National Institutes of Health, under award numbers 5R01 AR055966 (F.E.) and S10 RR027631 (D.S.P.), the National Center for Advancing Translational Sciences of the National Institutes of Health under award number UL1TR001105 (J.J.R.), the Pediatric Orthopaedic Society of North America and Texas Scottish Rite Hospital for Children (J.J.R.) and the US Army Medical Research Acquisition Activity under award W81XWH–11–1–0250 (D.A.S.). The content is solely the responsibility of the authors and does not necessarily represent the official views of the US National Institutes of Health or US government.

© 2014 Nature America, Inc. All rights reserved.

AUTHOR CONTRIBUTIONS

F.E. and J.d.l.C.N. designed the study; J.d.l.C.N., A.J.M., S.U., G.V., K.O., J.J.R., D.A.S., S.R.B., D.G., J.S.N. performed experiments; J.d.l.C.N., D.S.P., J.S.N. and F.E. collected and analyzed data; S.J. provided reagents; F.E. and J.d.l.C.N. wrote the manuscript.

COMPETING FINANCIAL INTERESTS

The authors declare competing financial interests: details are available in the online version of the paper.

Reprints and permissions information is available online at http://www.nature.com/reprints/index.html.

1. Huson, S.M., Compston, D.A., Clark, P. & Harper, P.S. A genetic study of von Recklinghausen neurofibromatosis in south east Wales. I. Prevalence, fitness, mutation rate, and effect of parental transmission on severity. *J. Med. Genet.* **26**, 704–711 (1989).
2. Stevenson, D.A. *et al.* Approaches to treating NF1 tibial pseudarthrosis: consensus from the Children's Tumor Foundation NF1 Bone Abnormalities Consortium. *J. Pediatr. Orthop.* **33**, 269–275 (2013).
3. Elefteriou, F. *et al.* Skeletal abnormalities in neurofibromatosis type 1: approaches to therapeutic options. *Am. J. Med. Genet. A.* **149A**, 2327–2338 (2009).
4. Kuorilehto, T. *et al.* Decreased bone mineral density and content in neurofibromatosis type 1: lowest local values are located in the load-carrying parts of the body. *Osteoporos. Int.* **16**, 928–936 (2005).
5. Stevenson, D.A. *et al.* Bone mineral density in children and adolescents with neurofibromatosis type 1. *J. Pediatr.* **150**, 83–88 (2007).
6. Duman, O. *et al.* Bone metabolism markers and bone mineral density in children with neurofibromatosis type-1. *Brain Dev.* **30**, 584–588 (2008).
7. Vitale, M.G., Guha, A. & Skaggs, D.L. Orthopaedic manifestations of neurofibromatosis in children: an update. *Clin. Orthop. Relat. Res.* **401**, 107–118 (2002).
8. Stevenson, D.A. *et al.* Descriptive analysis of tibial pseudarthrosis in patients with neurofibromatosis 1. *Am. J. Med. Genet.* **84**, 413–419 (1999).
9. Neitzschman, H.R., Costelloe, C.M., Willis, R.B. & De Mouy, E.H. Radiology case of the month. Congenital bone disorder associated with deformity, fracture, and pseudoarthrosis. Congenital tibial dysplasia–neurofibromatosis type I (NF1). *J. La. State Med. Soc.* **153**, 119–121 (2001).
10. Ippolito, E., Corsi, A., Grill, F., Wientroub, S. & Bianco, P. Pathology of bone lesions associated with congenital pseudarthrosis of the leg. *J. Pediatr. Orthop. B* **9**, 3–10 (2000).
11. Stevenson, D.A. *et al.* Double inactivation of NF1 in tibial pseudarthrosis. *Am. J. Hum. Genet.* **79**, 143–148 (2006).
12. Kolanczyk, M. *et al.* Multiple roles for neurofibromin in skeletal development and growth. *Hum. Mol. Genet.* **16**, 874–886 (2007).
13. Sullivan, K., El-Hoss, J., Little, D.G. & Schindeler, A. JNK inhibitors increase osteogenesis in Nf1-deficient cells. *Bone* **49**, 1311–1316 (2011).
14. Lee, D.Y. *et al.* Disturbed osteoblastic differentiation of fibrous hamartoma cell from congenital pseudarthrosis of the tibia associated with neurofibromatosis type I. *Clin. Orthop. Surg.* **3**, 230–237 (2011).
15. Leskelä, H.V. *et al.* Congenital pseudarthrosis of neurofibromatosis type 1: impaired osteoblast differentiation and function and altered NF1 gene expression. *Bone* **44**, 243–250 (2009).
16. Wu, X. *et al.* Neurofibromin plays a critical role in modulating osteoblast differentiation of mesenchymal stem/progenitor cells. *Hum. Mol. Genet.* **15**, 2837–2845 (2006).
17. Kühnisch, J. *et al.* Multiscale, converging defects of macro-porosity, microstructure and matrix mineralization impact long bone fragility in NF1. *PLoS ONE* **9**, e86115 (2014).
18. Elefteriou, F. *et al.* ATF4 mediation of NF1 functions in osteoblast reveals a nutritional basis for congenital skeletal dysplasiae. *Cell Metab.* **4**, 441–451 (2006).
19. Rhodes, S.D. *et al.* Hyperactive transforming growth factor-β1 signaling potentiates skeletal defects in a neurofibromatosis type 1 mouse model. *J. Bone Miner. Res.* **28**, 2476–2489 (2013).
20. Seitz, S. *et al.* High bone turnover and accumulation of osteoid in patients with neurofibromatosis 1. *Osteoporos. Int.* **21**, 119–127 (2010).
21. Johnson, K. *et al.* Linked deficiencies in extracellular PP_i and osteopontin mediate pathologic calcification associated with defective PC-1 and ANK expression. *J. Bone Miner. Res.* **18**, 994–1004 (2003).
22. Terkeltaub, R.A. Inorganic pyrophosphate generation and disposition in pathophysiology. *Am. J. Physiol. Cell Physiol.* **281**, C1–C11 (2001).
23. Macrae, V.E. *et al.* Inhibition of PHOSPHO1 activity results in impaired skeletal mineralization during limb development of the chick. *Bone* **46**, 1146–1155 (2010).
24. Harmey, D. *et al.* Concerted regulation of inorganic pyrophosphate and osteopontin by *Akp2*, *Enpp1*, and *Ank*: an integrated model of the pathogenesis of mineralization disorders. *Am. J. Pathol.* **164**, 1199–1209 (2004).
25. Addison, W.N., Azari, F., Sorensen, E.S., Kaartinen, M.T. & McKee, M.D. Pyrophosphate inhibits mineralization of osteoblast cultures by binding to mineral, up-regulating osteopontin, and inhibiting alkaline phosphatase activity. *J. Biol. Chem.* **282**, 15872–15883 (2007).
26. Sowa, H., Kaji, H., Yamaguchi, T., Sugimoto, T. & Chihara, K. Activations of ERK1/2 and JNK by transforming growth factor beta negatively regulate Smad3-induced alkaline phosphatase activity and mineralization in mouse osteoblastic cells. *J. Biol. Chem.* **277**, 36024–36031 (2002).
27. Lian, N. *et al.* Transforming growth factor β suppresses osteoblast differentiation via the vimentin activating transcription factor 4 (ATF4) axis. *J. Biol. Chem.* **287**, 35975–35984 (2012).
28. Terkeltaub, R.A. *et al.* Bone morphogenetic proteins and bFGF exert opposing regulatory effects on PTHrP expression and inorganic pyrophosphate elaboration in immortalized murine endochondral hypertrophic chondrocytes (MCT cells). *J. Bone Miner. Res.* **13**, 931–941 (1998).
29. Alves, R.D., Eijken, M., Bezstarosti, K., Demmers, J.A. & van Leeuwen, J.P. Activin A suppresses osteoblast mineralization capacity by altering extracellular matrix composition and impairing matrix vesicle production. *Mol. Cell. Proteomics* **12**, 2890–2900 (2013).
30. Zhang, M. *et al.* Osteoblast-specific knockout of the insulin-like growth factor (IGF) receptor gene reveals an essential role of IGF signaling in bone matrix mineralization. *J. Biol. Chem.* **277**, 44005–44012 (2002).
31. Kyono, A., Avishai, N., Ouyang, Z., Landreth, G.E. & Murakami, S. FGF and ERK signaling coordinately regulate mineralization-related genes and play essential roles in osteocyte differentiation. *J. Bone Miner. Metab.* **30**, 19–30 (2012).
32. Hatch, N.E., Nociti, F., Swanson, E., Bothwell, M. & Somerman, M. FGF2 alters expression of the pyrophosphate/phosphate regulating proteins, PC-1, ANK and TNAP, in the calvarial osteoblastic cell line, MC3T3E1(C4). *Connect. Tissue Res.* **46**, 184–192 (2005).
33. Wang, H. *et al.* Overexpression of fibroblast growth factor 23 suppresses osteoblast differentiation and matrix mineralization *in vitro*. *J. Bone Miner. Res.* **23**, 939–948 (2008).
34. Liu, S., Tang, W., Zhou, J., Vierthaler, L. & Quarles, L.D. Distinct roles for intrinsic osteocyte abnormalities and systemic factors in regulation of FGF23 and bone mineralization in Hyp mice. *Am. J. Physiol. Endocrinol. Metab.* **293**, E1636–E1644 (2007).
35. Le, L.Q. & Parada, L.F. Tumor microenvironment and neurofibromatosis type I: connecting the GAPs. *Oncogene* **26**, 4609–4616 (2007).
36. Wang, W. *et al.* Local low-dose lovastatin delivery improves the bone-healing defect caused by Nf1 loss of function in osteoblasts. *J. Bone Miner. Res.* **25**, 1658–1667 (2010).
37. Wang, W. *et al.* Mice lacking Nf1 in osteochondroprogenitor cells display skeletal dysplasia similar to patients with neurofibromatosis type I. *Hum. Mol. Genet.* **20**, 3910–3924 (2011).
38. Ono, K. *et al.* The Ras-GTPase activity of neurofibromin restrains ERK-dependent FGFR signaling during endochondral bone formation. *Hum. Mol. Genet.* **22**, 3048–3062 (2013).
39. Lecanda, F., Avioli, L.V. & Cheng, S.L. Regulation of bone matrix protein expression and induction of differentiation of human osteoblasts and human bone marrow stromal cells by bone morphogenetic protein-2. *J. Cell. Biochem.* **67**, 386–396 (1997).
40. Schindeler, A. *et al.* Modeling bone morphogenetic protein and bisphosphonate combination therapy in wild-type and Nf1 haploinsufficient mice. *J. Orthop. Res.* **26**, 65–74 (2008).
41. Schindeler, A. *et al.* Distal tibial fracture repair in a neurofibromatosis type 1-deficient mouse treated with recombinant bone morphogenetic protein and a bisphosphonate. *J. Bone Joint Surg. Br.* **93**, 1134–1139 (2011).
42. Whyte, M.P. *et al.* Enzyme-replacement therapy in life-threatening hypophosphatasia. *N. Engl. J. Med.* **366**, 904–913 (2012).
43. Whyte, M.P. Physiological role of alkaline phosphatase explored in hypophosphatasia. *Ann. NY Acad. Sci.* **1192**, 190–200 (2010).
44. Yadav, M.C. *et al.* Enzyme replacement prevents enamel defects in hypophosphatasia mice. *J. Bone Miner. Res.* **27**, 1722–1734 (2012).
45. Yadav, M.C. *et al.* Dose response of bone-targeted enzyme replacement for murine hypophosphatasia. *Bone* **49**, 250–256 (2011).
46. Rodda, S.J. & McMahon, A.P. Distinct roles for Hedgehog and canonical Wnt signaling in specification, differentiation and maintenance of osteoblast progenitors. *Development* **133**, 3231–3244 (2006).
47. Zhu, Y. *et al.* Ablation of NF1 function in neurons induces abnormal development of cerebral cortex and reactive gliosis in the brain. *Genes Dev.* **15**, 859–876 (2001).
48. Sohn, P., Crowley, M., Slattery, E. & Serra, R. Developmental and TGF-β-mediated regulation of Ank mRNA expression in cartilage and bone. *Osteoarthritis Cartilage* **10**, 482–490 (2002).
49. Cailotto, F., Sebillaud, S., Netter, P., Jouzeau, J.Y. & Bianchi, A. The inorganic pyrophosphate transporter ANK preserves the differentiated phenotype of articular chondrocyte. *J. Biol. Chem.* **285**, 10572–10582 (2010).
50. Larizza, L., Gervasini, C., Natacci, F. & Riva, P. Developmental abnormalities and cancer predisposition in neurofibromatosis type 1. *Curr. Mol. Med.* **9**, 634–653 (2009).
51. Anticevic, D., Jelic, M. & Vukicevic, S. Treatment of a congenital pseudarthrosis of the tibia by osteogenic protein-1 (bone morphogenetic protein-7): a case report. *J. Pediatr. Orthop. B* **15**, 220–221 (2006).
52. Lee, F.Y. *et al.* Treatment of congenital pseudarthrosis of the tibia with recombinant human bone morphogenetic protein-7 (rhBMP-7). A report of five cases. *J. Bone Joint Surg. Am.* **88**, 627–633 (2006).
53. Fabeck, L., Ghafil, D., Gerroudj, M., Baillon, R. & Delince, P. Bone morphogenetic protein 7 in the treatment of congenital pseudarthrosis of the tibia. *J. Bone Joint Surg. Br.* **88**, 116–118 (2006).

© 2014 Nature America, Inc. All rights reserved.

ONLINE METHODS

Animals and drugs. All procedures were approved by the Vanderbilt University Medical Center Institutional Animal Care and Use Committee (IACUC). WT and *Col2-Nf1* KO mice were generated by crossing *Nf1*$^{flox/flox}$ mice and *Nf1*$^{flox/+}$; α1(II) collagen-Cre breeders[47,54]. *Nf1*$^{flox/flox}$ mice and *Nf1*$^{flox/flox}$ mice; α1(II) collagen-Cre mice were used as WT and KO, respectively. *Osx-Nf1* KO mice were generated by breeding doxycycline-fed *Osx-cre*; *Nf1*$^{flox/flox}$ mice with *Nf1*$^{flox/flox}$ breeders[47]. All mice were on a C57BL/6 background. Bone analyses were performed in 18-d-old or 2-month-old male and female mice, as indicated in figure legends. sALP-FcD10 (Asfotase Alfa, Alexion Pharmaceuticals) was described previously[55]. Briefly, mineral-targeting recombinant tissue-nonspecific alkaline phosphatase (ALP, sALP-FcD10) was produced in CHO cells by modifying the coding sequence of human *ALPL*. The GPI anchor sequence of the hydrophobic C-terminal domain of human ALPL was removed to generate a soluble, secreted enzyme (sALP). Then the human *ALPL* ectodomain sequence was extended with the coding sequence encoding the Fc region of human IgG1 (Fc). Finally the C terminus of the Fc region was extended with ten aspartic acid residues (D10). The dose of 8.2 mg kg^{-1} per day was selected because it was previously shown to be efficacious in short-term (16 days) efficacy study in *Alpl*$^{-/-}$ mice[55]. The specific activity of the lot used in the present study was 878 U mg^{-1}. sALP-FcD10 was administered subcutaneously for the periods of time indicated in the text.

Human subjects. The study was approved by the Institutional Review Board of the University of Texas Southwestern Medical Center, of the Rizzoli Orthopaedic Institute (Bologna, Italy) and of Vanderbilt University. The parents of the subjects provided informed consent. Bone tissues were obtained from 9 patients with NF1 and tibial pseudarthrosis (aged between 7 months and 18 years), and control samples were obtained from 6 children without NF1 who underwent surgery for congenital dysplasia of the hip without any other coexisting pathology (n = 3)[56] or scoliosis (n = 3) (aged between 3.3 and 17 years). Diagnosis of pseudarthrosis was based on radiographic and clinical findings. Diagnosis of NF1 was performed according to the criteria presented at the National Institutes of Health Consensus Development Conference on Neurofibromatosis (http://consensus.nih.gov/1987/1987Neurofibramatosis064html.htm).

Cell culture. Mouse BMSCs were extracted from long bones by spinning down diaphyses at 1,500 r.p.m. for 3 min. Cells were then counted, plated at a density of 1 × 10^6 cells/well (12-well plates) or 2 × 10^6 cells/well (6-well plates) and grown for 7 days in αMEM supplemented with 10% FBS, 100 IU ml^{-1} penicillin, 100 μg/ml streptomycin (Cellgro, Manassas, VA, USA). At day 7, differentiation and mineralization was induced by the addition of 50 μg/ml ascorbic acid and 10 mM β-glycerophosphate, and the medium was refreshed every 2–3 days. BMSC differentiation and mineralization were assessed by ALP activity and Alizarin red S staining, respectively, using standard protocols.

Primary chondrocytes were extracted from 4-day-old pup rib bones. The cartilaginous part of the rib was dissected and soft tissues removed, then digested by collagenase D (3 mg/ml, Roche, USA) and 0.25% trypsin/EDTA (EDTA) (Gibco, USA) in DMEM for 3 h. At confluence, 5 × 10 μl drops of concentrated cells (2 × 10^7 cells/ml) were plated in 6 wells. After 2 h of incubation, 2 ml of complete cell culture medium was delicately added. Cells were differentiated in DMEM supplemented with 10% FBS, 100 IU ml^{-1} penicillin, 100 μg ml^{-1} streptomycin, 50 μg ml^{-1} of ascorbic acid and 10 mM β-glycerophosphate.

Human cells extracted from bone marrow[56] or bone tissue were maintained in alpha MEM supplemented with 10% FBS, 100 U ml^{-1} penicillin, 0.1 mg ml^{-1} streptomycin at 37 °C in a 5% CO_2-humidified atmosphere. Cells from bone tissues were digested overnight with collagenase before plating. After 4 days, nonadherent cells were removed, and adherent bone cells were grown until confluence or passaged before RNA extraction.

Adenovirus infection of bone marrow stromal cells. BMSCs were isolated from *Nf1*$^{flox/flox}$ mice and seeded at a density of 1 × 10^6 cells/well in 12-well plates. At 40% confluence, cells were incubated in complete culture medium (α-MEM, 10% FBS and 100 IU ml^{-1} penicillin) containing either Ad5-CMV-GFP or Ad5-CMV-Cre (Vector development lab, Baylor College of Medicine) at 2.5 × 10^9 PFUs. After 2 days of incubation, the medium was refreshed with complete culture medium. *Nf1* recombination efficiency was determined according to Wang *et al.*[37].

Serum vitamin D, calcium and phosphate assays. Blood samples were collected from WT and *Osx-Nf1* KO mice at sacrifice. Vitamin D, phosphate and calcium concentration in mouse serum was determined using a 25OH-Vitamin-D ELISA Assay kit (Eagle Biosciences, cat# VID31-K01), a Phosphate Assay kit (BioVision, cat # k410-500) and a Calcium Assay kit (BioVision, cat# k380-250), respectively, according to the manufacturer's instructions.

PP_i and PC-1 assays. PP_i release in cell-conditioned medium (ePP_i) was measured radiometrically using differential adsorption on activated charcoal of uridine-diphospho-D-glucose [6-^{3}H] (Cat #NET1163250UC, PerkinElmer) as previously described[49,57,58]. Forty microliters of conditioned medium (or blank control) and 120 μl of assay solution (57 nM of Tris acetate, pH 7.6; 5.2 mM MgAc; 18.6 μM glucose 1,6-diphosphate (G1,6DP); 9 μM uridine-diphosphoglucose (UDPG); 4 μM β-nicotinamide adenine dinucleotide (NAD+); 0.136 U uridine-diphosphoglucose pyrophosphorylase (UDPGPP); 0.5 U phosphoglucomutase; 0.5 U glucose-6-phosphate dehydrogenase (G6PD); 0.02 μCi ^{3}H-UDPG) were incubated at 37 °C for 1 h and then adsorbed on 200 μl of charcoal for 10 min on ice. After centrifugation at 14,000 r.p.m. for 10 min, 100 μl of the supernatant was transferred into a vial containing 5 ml of Bio-safe II for radioactivity count. PP_i levels were normalized by protein concentration in cell lysates in each well. Measurements were performed in triplicate and similar results were obtained from at least 3 independent experiments.

ENPP1 activity was determined using 1.5 mM of the synthetic chromogenic substrate thymidine 5′-monophosphate *p*-nitrophenyl ester in reaction buffer (100 mM Tris/HCl, pH 8.0, 130 mM NaCl, and 15 mM $MgCl_2$) incubated at 37 °C for 30 min. The reaction was terminated by the addition of 50 μl 4 N NaOH. Product formation was monitored by measurement of absorbance at 405 nm. ENPP1 activity in each well was normalized by cell number. Measurements were performed in triplicate and from at least 3 independent experiments.

RT-qPCR and genomic PCR. Total RNA was extracted using TRIzol (Invitrogen, Grand Island, NY, USA), and cDNAs were synthesized from 1 μg of RNA following DNase I treatment using the high-capacity cDNA reverse-transcription kit (Applied Biosystems, USA). Quantitative PCR (qPCR) was performed by using TaqMan or SYBR green gene expression assays. The probe and primer sets for mouse *Runx2* (Mm00501578_m1); *Alpl* (Mm00475834_m1); *Ank* (Mm00445047_m1); *Enpp1* (Mm00501097_m1); *Spp1* (Mm00436767_m1), *Igf1* (Mm01228180_m1), human *ANKH* (Hs00219798_m1) and human *ENPP1* (Hs01054040_m1) and the normalizers *Hprt* (Mm00446968_m1); human *GAPDH* (Hs99999905_m1) were obtained from Applied Biosystems (Foster City, CA, USA). The SYBR green primers were *Spp1* (forward; CTCCTTGCGCCACAGAATG, reverse; TGGGCAACAGGGATGACA), *Nf1* (forward; GTATTGAATTGAAGCACC TTTGTTTGG, reverse; CTGCCCAAGGCTCCCCCAG); *Bglap* (forward; ACCCTGGCTGCGCTCTGTCTCT, reverse; GATGCGTTTGTAGGCGGTC TTCA) and *Col1a1* (forward; GACATCCCTGAAGTCAGCTGC, reverse; TCCCTTGGGTCCCTCGAC). Specificity of amplification was verified by the presence of a single peak on the dissociation curve. Amplification conditions are available upon request. Measurements were performed in triplicate and from at least 3 independent experiments.

For genotyping, genomic DNA was isolated from tail tips by sodium hydroxide digestion, and PCR was performed using primers P1, P2 and P4, as described by Zhu *et al.*[47]. The *Col2a1-cre* transgene was detected using the fwd: GAGTT GATAGCTGGCTGGTGGCAGATG and reverse: TCCTCCTGCTCCTAGGG CCTCCTGCAT primers.

Western blot analyses. Whole cell lysates were separated by SDS-PAGE electrophoresis according to standard protocols. Nitrocellulose membranes were probed with the indicated antibody using standard protocols (monoclonal anti-β-actin antibody (Sigma cat# AC-74, dilution 1:5,000), anti-pSmad1/5 antibody (Cell Signaling cat#9516S, dilution 1:1,000), anti-Smad1/Smad5 antibody (Abcam cat# ab75273, dilution 1:1,000), anti ENPP1/PC-1 (Aviva Systems Biology,

© 2014 Nature America, Inc. All rights reserved.

cat# OAEB02445, dilution 1:500) and anti-ANK (Origen, cat# TA325111, dilution 1:1,000).

Histology. Static histomorphometry measurements were performed as previously described in accordance with standard nomenclature[59], using the Bioquant Analysis System (Nashville, TN, USA) on 5 μm undecalcified methymethacrylate sections. Calcified cartilage BV/TV was measured in the growth plate hypertrophic region following von Kossa and van Gieson staining.

X-rays and μCT analyses. Radiographs were obtained using a digital cabinet X-ray system (LX-60, Faxitron X-Ray, USA). μCT analyses were performed using a Scanco μCT 40 system (Scanco Medical, Bassersdorf, Switzerland). Tomographic images were acquired at 55 kVp and 145 mA with an isotropic voxel size of 12 μm and at an integration time of 250 ms with 500 projections collected per 180° rotation.

Raman spectroscopy. Sensitive to the vibrational modes of chemical bonds, Raman spectroscopy (RS) characterizes the biochemical properties of bone tissue, namely mineral-to-collagen ratio (MCR) and crystal structure. Using midshaft vessel perforations as landmarks, spectra were obtained from cortical bone of the femur with 5 accumulations of 20 s exposures to a 20-mW, near-infrared laser (785 nm) at a spot size of ~1.5 μm in diameter. Spectra were processed via least-squares modified polynomial fit to suppress background fluorescence[60] and smoothed for noise using a second-order Savitsky-Golay filter[61]. Raman shift calibration was accomplished using a neon lamp and a silicon standard. Silicon standard measurements before and after data acquisition ensured wave number consistency across bones. Spectral intensities for known Raman peaks and peak ratios were extracted using custom Matlab software (Mathworks, Natick, MA) to measure mineralization as ν1 phosphate (symmetrical stretching at ~960 cm^{-1}) per proline (ring at ~854 cm^{-1}) and crystallinity (crystal grain size and perfection) as the inverse full width at half maximum intensity of the ν1 phosphate peak).

Biomechanical testing. Hydrated samples were tested in three-point bending with a span of 8 mm at a rate of 3 mm min^{-1} (ref. 62). Force and displacement were measured from a 100 N load cell and from the linear variable displacement transformer of the material testing system (Dynamight 8841, Instron, Canton, OH). Structural properties were extracted from force-displacement curves by custom Matlab algorithms (Mathworks, Natick, MA). Material properties were calculated by accounting for structure by using cross-sectional area and moment of inertia as measured by μCT.

Statistical analyses. Depending on whether data per group passed the Shapiro-Wilk normality test or whether standard deviations were not different among the groups (Bartlett's test), one-way analysis of variance (ANOVA) or the Kruskal-Wallis Test (nonparametric) was used to determine whether differences existed in μCT -, Raman- and biomechanical-derived properties among the experimental groups. When differences existed at $P < 0.05$, *post hoc* pair-wise comparisons were tested for significance in which the P value was adjusted ($P_{adj} < 0.05$) by Holm-Sidak's method or Dunn's method (nonparametric). Statistical analysis was performed using GraphPad PRISM (v6.0a, La Jolla, CA). Data are provided as mean ± s.d. No statistical method was used to predetermine sample size. The investigators were blinded to allocation during experiments and outcome assessment. The experiments were not randomized.

54. Ovchinnikov, D.A., Deng, J.M., Ogunrinu, G. & Behringer, R.R. Col2a1-directed expression of Cre recombinase in differentiating chondrocytes in transgenic mice. *Genesis* **26**, 145–146 (2000).
55. Millán, J.L. *et al.* Enzyme replacement therapy for murine hypophosphatasia. *J. Bone Miner. Res.* **23**, 777–787 (2008).
56. Granchi, D. *et al.* Biological basis for the use of autologous bone marrow stromal cells in the treatment of congenital pseudarthrosis of the tibia. *Bone* **46**, 780–788 (2010).
57. Terkeltaub, R., Rosenbach, M., Fong, F. & Goding, J. Causal link between nucleotide pyrophosphohydrolase overactivity and increased intracellular inorganic pyrophosphate generation demonstrated by transfection of cultured fibroblasts and osteoblasts with plasma cell membrane glycoprotein-1. Relevance to calcium pyrophosphate dihydrate deposition disease. *Arthritis Rheum.* **37**, 934–941 (1994).
58. Cailotto, F. *et al.* Inorganic pyrophosphate generation by transforming growth factor-β-1 is mainly dependent on ANK induction by Ras/Raf-1/extracellular signal-regulated kinase pathways in chondrocytes. *Arthritis Res. Ther.* **9**, R122 (2007).
59. Parfitt, A.M. *et al.* Bone histomorphometry: standardization of nomenclature, symbols, and units. Report of the ASBMR Histomorphometry Nomenclature Committee. *J. Bone Miner. Res.* **2**, 595–610 (1987).
60. Lieber, C.A. & Mahadevan-Jansen, A. Automated method for subtraction of fluorescence from biological Raman spectra. *Appl. Spectrosc.* **57**, 1363–1367 (2003).
61. Maher, J.R., Takahata, M., Awad, H.A. & Berger, A.J. Raman spectroscopy detects deterioration in biomechanical properties of bone in a glucocorticoid-treated mouse model of rheumatoid arthritis. *J. Biomed. Opt.* **16**, 087012 (2011).
62. Makowski, A.J. *et al.* The loss of activating transcription factor 4 (ATF4) reduces bone toughness and fracture toughness. *Bone* **62**, 1–9 (2014).

© 2014 Nature America, Inc. All rights reserved.

doi:10.1038/nm.3583